Proceedings of the 6th International Conference on Biological Engineering and Medical Science
DOI: 10.54254/2753-8818/2026.36010

Roles of LTF and HAMP in Neuronal Ferroptosis in Alzheimer's Disease Cell Model

Jiaxuan He

Shanghai Starriver Bilingual School, Shanghai, China
18301936451@163.com

Abstract. Dysregulation of iron homeostasis and ferroptosis is increasingly implicated in Alzheimer's disease (AD) pathology. Lactotransferrin (LTF) and hepcidin (HAMP) are key regulators of neuronal iron metabolism, but their role in AD-related ferroptosis remains unclear. Bioinformatics analysis of hippocampal RNA-sequencing data from AD patients and healthy controls identified differentially expressed genes (DEGs) associated with iron metabolism. SH-SY5Y cells were treated with Aβ oligomers to establish AD cell models and further subjected to siRNA-mediated knockdown of LTF or HAMP. Ferroptosis was evaluated using Fe^{2+} accumulation, lipid reactive oxygen species (ROS), mitochondrial morphology, MDA/GSH levels, and the expression of core ferroptosis regulators (GPX4, SLC7A11, ACSL4). Cell viability, LDH release, and apoptosis were also assessed. Bioinformatics analysis revealed LTF and HAMP as key DEGs related to iron homeostasis, potentially linked to ferroptosis in AD. In vitro, Aβ treatment decreased LTF and HAMP expression, induced Fe^{2+} accumulation, oxidative stress, mitochondrial damage, and ferroptotic cell death. Knockdown of LTF or HAMP further exacerbated these effects, while treatment with the ferroptosis inhibitor Fer-1 partially restored cellular homeostasis and viability. The data suggest a regulatory role of LTF and HAMP in neuronal ferroptosis. Notably, hyper-expression of LTF and HAMP observed in post-mortem AD hippocampal samples likely reflects compensatory negative feedback mechanisms in late-stage disease. LTF and HAMP act as protective modulators against neuronal ferroptosis in AD. Their early downregulation promotes iron overload and oxidative stress, whereas compensatory upregulation in vivo delays ferroptosis. Targeting LTF and HAMP-mediated pathways may provide novel therapeutic strategies for mitigating AD progression.

Keywords: Alzheimer's disease, LTF, HAMP, ferroptosis, SH-SY5Y, iron homeostasis

1. Introduction

Alzheimer's disease (AD) is a severe progressive neurodegenerative disease characterized by the accumulation of amyloid β (Aβ) plaque and hyperphosphorylation of tau [1, 2]. In 2023, approximately 416 million people worldwide were estimated to be along the AD continuum (dementia, prodromal, or preclinical stages), accounting for about 22% of the global population with an age of 50 or more [3]. According to mortality analyses, during 2020-2021, the global age-standardized death rate of dementias was 24.9 per 100000 people, ranking the 7th largest cause of

DOI: 10.54254/2753-8818/2026.36010

death among all 175 Level-3 causes in the Global Burden of Disease Study 2021 [4]. Moreover, the population living with dementia is predicted to increase significantly in the future decades due to population growth and aging [5]. The vast and expanding patient population, together with the considerable mortality burden, poses a major global health challenge and highlights the urgent need for innovating strategies to prevent and treat AD.

According to the widely-recognized amyloid cascade hypothesis, Aβ accumulation is the earliest characterizing feature of AD and the pivotal inducer of the later progression of the disease, such as p-tau pathology [6]. Consequently, neuronal death and neuroinflammation occur, ultimately leading to severe memory loss in affected patients [7, 8]. Because this cascade is highly complex, elucidating the mechanisms by which Aβ drives downstream pathological events is critical for the development of methods for prevention and cure targeting these pathways. In response to this need to discover the biological pathways of AD, scientists have expanded on the amyloid cascade hypothesis, identifying key genes and signaling pathways contributing to the progression of the disease. However, there are still many parts missing in the hypothesis due to the complexity of AD pathogenesis, including the regulators of neuronal loss.

Among the proposed explanations, ferroptosis—a regulated, iron-dependent type of non-apoptotic cell death—has emerged [9]. Disruption of iron homeostasis, a key metabolic process in the central nervous system (CNS), can trigger ferroptosis and has been shown to be prevalent in neurodegenerative diseases like AD and Parkinson's disease [10-14]. In AD, iron overload acts both as an important regulator of ferroptosis and a driver of AD pathology [15]. Its leading to oxidative stress is believed to be a major cause of cognitive degradation, consistent with the mechanism of ferroptotic cell death [16]. Therefore, elucidating how neuronal ferroptosis is regulated, particularly at the gene expression level, is critical for understanding the basis of neuronal loss in AD. However, specific genes mediating ferroptosis in AD remain insufficiently characterized.

There are some well-known ferroptosis markers, including GPX4, SLC7A11, ACSL4, and so on. GPX4, the gene coding for an enzyme that reduces lipid peroxidation, is one of the most important genes regulating ferroptosis with its activation disrupting the entire pathway [10, 17]. SLC7A11, the antiporter of cystine/glutamate, inhibits ferroptosis through its expression by promoting glutathione (GSH) synthesis and thus facilitating GPX4-driven detoxification of lipid peroxides [18]. Glutathione (GSH) levels can be tested by 5,5'-dithiobis-2-nitrobenzoic acid (DTNB) as they react to form a yellow-colored TNB compound, and thus the concentration of it can be obtained through spectrophotometry and calculation [19]. GSH reduces lipid peroxides, so it acts as a countering force against ferroptosis, and a decreased level of it shows greater levels of ferroptosis [10, 20]. In contrast, ACSL4, a ferroptosis determinant gene, facilitates the incorporation of oxidation-prone polyunsaturated phospholipids (PUFA-PLs) into membranes, promoting lipid peroxidation and driving ferroptotic cell death [21]. An increase in GPX4 and SLC7A11 expression together with a decrease in ACSL4 suggests ferroptosis inhibition, whereas the opposite pattern indicates ferroptosis activation [22, 23].

This work aims to identify ferroptosis-related genes through bioinformatics analysis of RNA-seq data from AD patients (GEO dataset GSE236562) and to investigate their contribution to neuronal loss in AD using an SH-SY5Y cell-based AD model combined with molecular biology techniques. The findings are expected to provide new insights into neuronal ferroptosis mechanisms and potential cures for AD.

DOI: 10.54254/2753-8818/2026.36010

2. Materials and methods

2.1. Acquiring the database for differentially-expressed genes (DEGs)

RNA-seq data were obtained from the Gene Expression Omnibus (GEO) database, accession number GSE236562 (https://www.ncbi.nlm.nih.gov/geo/query/acc.cgi?acc=GSE236562). This dataset contains 32 RNA-seq samples derived from the hippocampus (HP) or cortex of human brain with or without SARS-CoV-2 infection. For the present study, eight hippocampal samples from subjects not affected by SARS-CoV-2 were selected for downstream analysis of DEGs between AD patients and age-matched normal controls. Detailed sample accession information is provided in Table 1.

Table 1. Information on human samples and the tested regions of the RNA sequences

Group	Accession	Tissue	Brain region	Age	Sex
Control	GSM7552865	Brain	HP	73	Male
Control	GSM7552866	Brain	HP	82	Male
Control	GSM7552868	Brain	HP	72	Female
Control	GSM7552873	Brain	HP	77	Female
AD	GSM7552875	Brain	HP	66	Female
AD	GSM7552877	Brain	HP	95	Male
AD	GSM7552879	Brain	HP	91	Female
AD	GSM7552882	Brain	HP	77	Male

2.2. Bioinformatics analysis

Bioinformatics analyses were performed using the platform *Bioinformatics.com.cn* (https://www.bioinformatics.com.cn, last accessed 10 Dec 2024), which integrates commonly used R packages for transcriptomic analysis and visualization (including limma, ggplot2, and clusterProfiler). Differentially expressed genes (DEGs) between the AD and control groups were identified using the limma package, with thresholds set at $|\log_2 FC| > 2$ and adjusted $P < 0.05$. An enhanced volcano plot was generated to visualize the DEGs. A heatmap and protein–protein interaction (PPI) network were constructed using normalized mean counts. Global expression differences between samples were further assessed via 3D UMAP. Functional enrichment of DEGs was performed through the clusterProfiler package with reference to the KEGG and Gene Ontology (GO) databases. The primary aim of these analyses was to identify ferroptosis-related genes with significant expression changes in AD.

2.3. Cell culture and model construction

SH-SY5Y human neuroblastoma cells (iCell, iCell-h187) were cultured in Dulbecco's Modified Eagle Medium (DMEM) supplemented with 10% fetal bovine serum (FBS) and 1% penicillin–streptomycin at 37 °C in a humidified atmosphere containing 5% CO_2. Cells were passaged every 2–3 days and used for experiments at 70–80% confluence. To establish AD-like cell models, SH-SY5Y cells were treated with 10 μM Aβ42 oligomers (Abcam, ab120301) for 24 hours. For ferroptosis-inhibited models, cells were pretreated with 5 μM Ferrostatin-1 (Fer-1) for 30 minutes before Aβ42 exposure.

DOI: 10.54254/2753-8818/2026.36010

Five experimental groups were established: (1) normal control cells, (2) AD-like cell models treated with 10 μM Aβ42 oligomers (Abcam, ab120301) for 24 hours, (3) ferroptosis-inhibited AD models pretreated with 5 μM Ferrostatin-1 for 30 minutes before Aβ42 exposure, and (4–5) target gene–knockdown AD models. For each gene, three siRNAs were initially tested, and the one achieving the most effective knockdown was used. Forty-eight hours post-transfection, knockdown efficiency was evaluated at mRNA levels by qRT-PCR, with GAPDH as the internal control.

2.4. Quantification of gene expression

The expression levels of target genes and ferroptosis-related genes GPX4, SLC7A11, and ACSL4 were measured in all groups using qRT-PCR and Western blotting. Total RNA was extracted using a commercial kit and reverse-transcribed into cDNA following the manufacturer's instructions. qRT-PCR was performed with gene-specific primers, and relative expression levels were calculated using the $2^{-\Delta\Delta Ct}$ method, with GAPDH serving as the internal control. For protein analysis, cells were lysed, and equal amounts of protein were separated by SDS-PAGE and transferred to PVDF membranes. Membranes were probed with specific primary antibodies, followed by HRP-conjugated secondary antibodies. An enhanced chemiluminescence detection system was used for protein bands visualization.

2.5. CCK-8 assay

Cell proliferation and viability were assessed using the Cell Counting Kit-8 (CCK-8, Dojindo, CK04). Each cell line was seeded into 96-well plates in triplicate and incubated at 37 °C with 5% CO_2 for 24, 48, and 72 hours. At each time point, 10 μL of CCK-8 solution was added to each well and incubated for 4 hours. A microplate reader was used for obtaining the absorbance at 450 nm, from which cell viability was calculated relative to the control group.

2.6. Flow cytometry

Cell apoptosis was assessed with the Annexin V-FITC/PI apoptosis detection kit (Beyotime, C1062S). For each sample, 50,000–100,000 cells were resuspended in 195 μL Annexin V-FITC binding buffer, then 5 μL Annexin V-FITC and 10 μL propidium iodide (PI) were added. After incubation in the dark for 15 minutes at room temperature, apoptosis rates were measured by flow cytometry. Early apoptotic cells were Annexin V-positive and PI-negative, whereas late apoptotic/necrotic cells were double-positive.

2.7. Lactate dehydrogenase (LDH) release assay

Cytotoxicity was evaluated by measuring LDH release using an LDH detection kit (MLBio, Ml092588). Cell culture supernatants were collected from each cell line, and LDH reaction mixture was added according to the manufacturer's instructions. After incubation for 30–60 minutes at room temperature, absorbance was assessed to quantify LDH levels, which reflect membrane damage and cell death.

2.8. Measurement of reactive oxygen species (ROS) levels

Lipid ROS levels in the different cell lines were analyzed using the MitoSO™ Red mitochondrial peroxidation detection kit (Beyotime, S0061S). Cells were incubated with the staining reagent at

DOI: 10.54254/2753-8818/2026.36010

37 °C for 1 hour, and the stained lipid ROS were visualized under a fluorescence microscope. Fluorescence intensity was quantified to determine the oxidized/reduced lipid ROS ratio.

10 μM DCFH-DA (Beyotime, S0033S) was used for general intracellular ROS level assessment. Cells were stained according to the manufacturer's instructions and analyzed by flow cytometry. Detection used a 488 nm excitation wavelength and 525 ± 20 nm emission wavelength. Data were analyzed using FlowJo software, and the oxidized/reduced ROS ratio was calculated.

2.9. Fe^{2+} levels measurement

Intracellular Fe^{2+} levels were detected using FerroOrange (Servicebio, G1727-100T). Cells were incubated with the FerroOrange reagent at 37 °C for 30 minutes, and Fe^{2+} accumulation was visualized under a fluorescence microscope. Fluorescence intensity was quantified to assess labile Fe^{2+} content.

2.10. Measurement of MDA and GSH levels

Malondialdehyde (MDA) levels were measured using the mlbio MDA detection kit (mlsh0387). MDA reacted with thiobarbituric acid (TBA) to form a red compound, and absorbance was measured at 532 nm and 600 nm to calculate MDA concentration.

Glutathione (GSH) levels were determined using the mlbio GSH detection kit (ml076449). GSH reacts with 5,5'-dithiobis-(2-nitrobenzoic acid) (DTNB) to produce a yellow-colored TNB compound, and the concentration was quantified by spectrophotometry. As a key antioxidant, GSH reduces lipid peroxides and counteracts ferroptosis; decreased GSH levels indicate enhanced ferroptotic activity.

2.11. Mitochondrial morph observation

Mitochondrial ultrastructure was examined by transmission electron microscopy (TEM). Cells were fixed, processed, and observed to assess changes in mitochondrial morphology and density associated with ferroptosis.

3. Results

3.1. Bioinformatics analysis identifies LTF and HAMP as candidate target genes

Bioinformatics analysis of hippocampal RNA-seq samples from database GSE236562 (Table 1) identified significantly differentially expressed genes (DEGs) between AD patients and age-matched controls. Volcano plot analysis (Figure 1A) was used to select the 20 most significant DEGs with adjusted $P < 0.05$ and $|\log_2 FC| > 2$. The gene IDs, *adjusted P-values,* and fold changes ($\log_2 FC$) are summarized in Table 2. Among these 20 DEGs, four genes (CYP4F29P, SIGLEC10-AS1, LOC110091776, and LOC112267910) were identified as non-protein-coding based on the NCBI gene database (https://www.ncbi.nlm.nih.gov/gene). The remaining 16 mRNAs were used for further analysis. Heat map visualization (Figure 1B) revealed that ABCC12, FREM3, MAFIP, and SV2C were downregulated, whereas LTF, HAMP, FPR1, MYO1G, CCL2, SERPINA3, SOCS3, SECTM1, SERPINA5, NGFR, SPP1, and CD163 were upregulated in AD samples relative to controls.

DOI: 10.54254/2753-8818/2026.36010

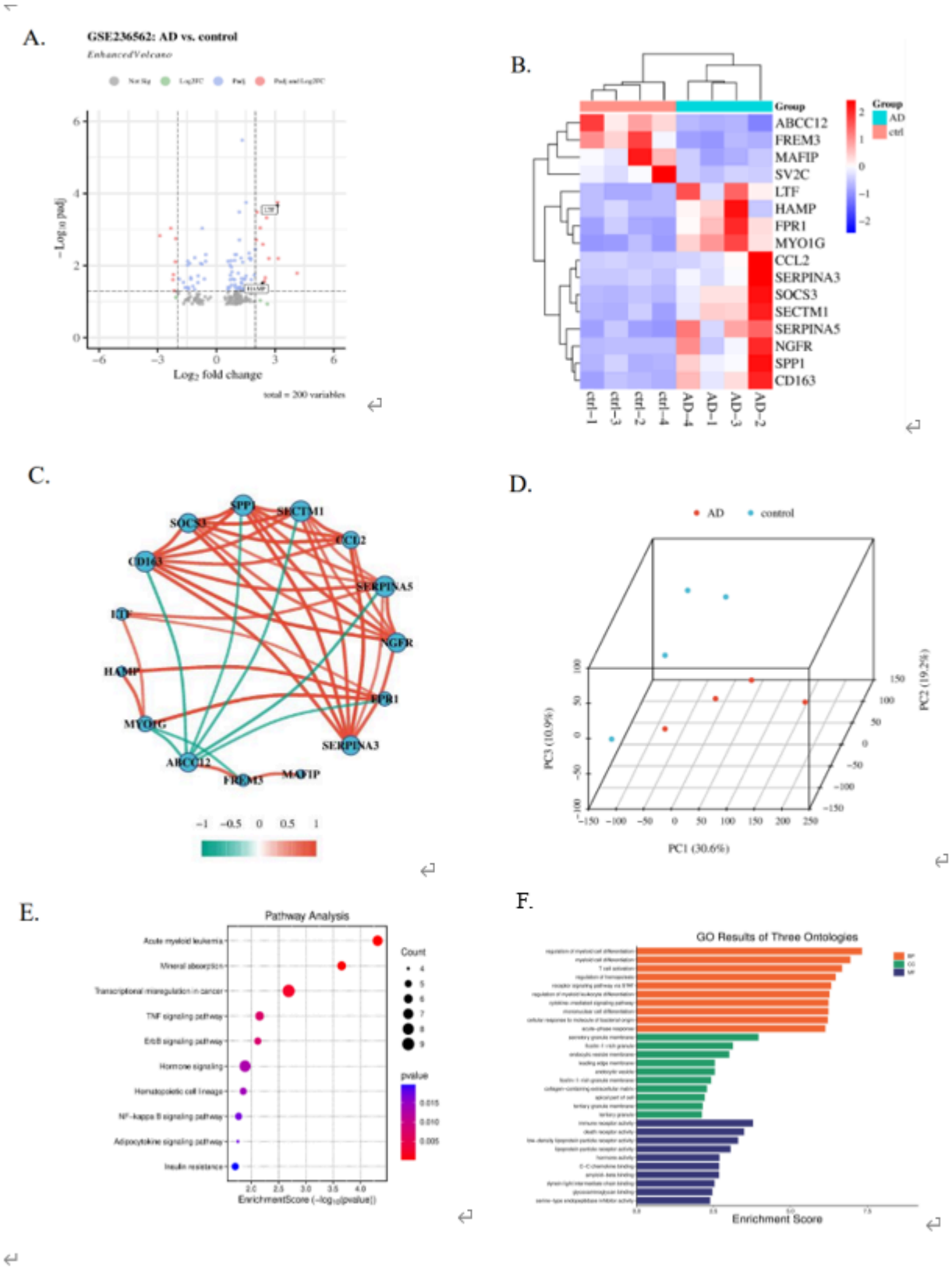

Figure 1. Bioinformatics analysis of DEGs in human hippocampus between AD and normal control. (A) Volcano plot illustrating the top 200 DEGs identified from RNA sequencing data. (B) Heat map displaying the top 16 DEGs. (C) Protein-protein interaction (PPI) network depicting the correlations

DOI: 10.54254/2753-8818/2026.36010

among DEGs. (D) The UMAP visualization of genomic mRNA sequences from the samples obtained from the GEO database. (E) KEGG pathway enrichment analysis of genomic mRNA sequences. (F) Gene Ontology (GO) enrichment analysis of mRNA expression profiles

Table 2. Significantly Top 20 DEGs in hippocampus between AD and control (AD vs. control)

Gene ID	Symbol	log2FC	*P-value*
12	SERPINA3	3.163	0.00636584
2357	FPR1	2.084	0.00032774
4057	LTF	3.121	0.00017735
4804	NGFR	2.686	0.00636584
5104	SERPINA5	2.377	0.00257853
6347	CCL2	4.126	0.01632044
6398	SECTM1	2.5	0.02176247
6696	SPP1	2.239	0.00090223
9021	SOCS3	2.566	0.00047022
9332	CD163	2.552	0.00032774
22987	SV2C	-2.22	0.02459884
54055	CYP4F29P	-2.891	0.00149038
57817	HAMP	2.456	0.0271778
64005	MYO1G	2.033	0.00194006
94160	ABCC12	-2.102	0.00783355
166752	FREM3	-2.334	0.00092495
727764	MAFIP	-2.2	0.01791294
100129083	SIGLEC10-AS1	2.011	0.037483
110091776	LOC110091776	-2.157	0.04988458
112267910	LOC112267910	-2.076	0.00179464

The protein-protein interaction (PPI) network (Figure 1C) illustrates potential correlations among the 16 protein-coding DEGs. Notably, LTF and HAMP both interact with FPR1, and both genes are involved in iron transport and homeostasis, suggesting a potential regulatory mechanism. Based on this observation, we hypothesize that LTF and HAMP may contribute to ferroptosis in AD neurons. Overall genomic differences in mRNA expression between AD and control samples are depicted in the 3D UMAP plot (Figure 1D), which shows a clear separation between AD and control groups, indicating substantial transcriptional dysregulation in AD. KEGG pathway enrichment analysis (Figure 1E) demonstrates that several DEGs are involved in pathways related to mineral absorption and iron metabolism, further supporting the connection between altered iron homeostasis and AD pathology. GO enrichment analysis (Figure 1F) highlights differences in biological processes, cellular components, and molecular functions, including those associated with iron ion transport, oxidative stress response, and cellular metal ion homeostasis.

Among the DEGs, LTF (lactotransferrin/lactoferrin) and HAMP (hepcidin) were identified as potential key regulators of iron homeostasis, the potential factors in ferroptosis implicated in AD pathology.

DOI: 10.54254/2753-8818/2026.36010

3.2. Functional validation of LTF and HAMP in SH-SY5Y cell models

Figure 2A shows the effects of the different siRNAs on SH-SY5Y cells. For LTF, LTF-1265 siRNA markedly reduced LTF expression, LTF-1645 caused a modest reduction, and LTF-1929 unexpectedly increased LTF levels. Therefore, LTF-1265 was selected for subsequent experiments. For HAMP, HAMP-54 and HAMP-154 significantly decreased HAMP expression, whereas HAMP-273 had minimal effect. HAMP-154 was chosen for further studies due to its higher knockdown efficiency.

To elucidate the functional roles of LTF and HAMP in AD and their potential involvement in ferroptotic pathways, we established several SH-SY5Y cell line groups: 1) Ctrl, SY5Y cell line; 2) Aβ, SY5Y AD cell model; 3) Aβ+Fer-1, AD cell model treated with Fer-1 (ferroptosis inhibitor); 4) Aβ+siLTF, AD cell model transfected with LTF-1265 siRNA; 5) Aβ+siHAMP, AD cell model transfected with HAMP-54 siRNA. Figures 2B and 2C compare LTF and HAMP expression across normal SH-SY5Y cells, AD cell models, AD models treated with Fer-1, and AD models with targeted knockdown of LTF or HAMP. Both genes exhibited reduced expression in AD cell models relative to controls, indicating that Aβ exposure downregulates LTF and HAMP, which may contribute to early AD pathogenesis. Treatment with Fer-1 partially restored LTF and HAMP expression, suggesting that upregulation of these genes may participate in the ferroptosis-inhibitory mechanism of Fer-1.

Interestingly, knockdown of one gene also reduced the expression of the other, suggesting a potential regulatory interaction between LTF and HAMP, although the underlying mechanism remains to be investigated. These results suggest a cross-regulation of LTF and HAMP and highlight their possible roles in neuronal ferroptosis in AD, warranting further exploration in future studies.

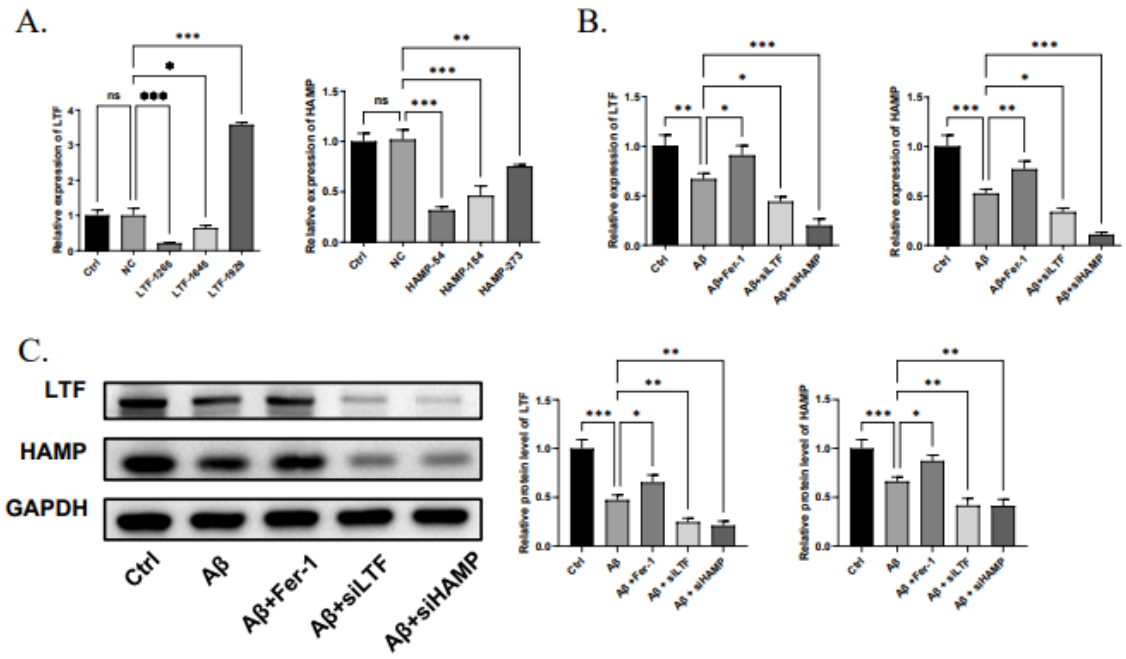

Figure 2. The Expression of LTF and HAMP in groups. (A) qRT-PCR analysis of LTF and HAMP expression after the intervention of three different siRNAs. (B) qRT-PCR results highlighting relative LTF and HAMP expression in groups. (C) Western blot showing relative protein levels of LTF and HAMP, with GAPDH as loading control

DOI: 10.54254/2753-8818/2026.36010

3.3. Effects of LTF and HAMP on cell viability and apoptosis

To investigate the roles of LTF and HAMP in neuronal survival, we assessed cell proliferation, cytotoxicity, and apoptosis in SH-SY5Y-derived AD cell models using CCK-8 assays, LDH release assays, and flow cytometry, respectively. Figure 3A shows that AD model cells (Aβ-treated) exhibited significantly lower OD values compared with normal SH-SY5Y cells, indicating impaired proliferation in early AD. This decrease in proliferation correlates with reduced expression of LTF and HAMP, suggesting that their downregulation negatively affects cell growth. Treatment with the ferroptosis inhibitor Fer-1 partially restored cell viability, supporting a protective role of LTF and HAMP against ferroptotic damage. Furthermore, siRNA-mediated knockdown of LTF or HAMP caused an additional reduction in OD values, reinforcing their positive contribution to neuronal proliferation. Figure 3B shows that LDH release, an indicator of cell membrane damage and cytotoxicity, was significantly increased in AD models with LTF or HAMP knockdown compared with control cells, highlighting the protective effect of these genes. Flow cytometry analysis (Figures 3C and 3D) confirmed these observations, demonstrating elevated apoptosis rates in AD models following LTF or HAMP knockdown. Conversely, Fer-1 treatment reduced apoptosis, indicating that inhibition of ferroptosis mitigates cell death.

Taken together, these results indicate that reduced LTF and HAMP expression in early AD contributes to neuronal death, and further suppression of these genes amplifies cytotoxicity and apoptosis. Fer-1-mediated restoration further supports their role in ferroptosis-dependent neuroprotection.

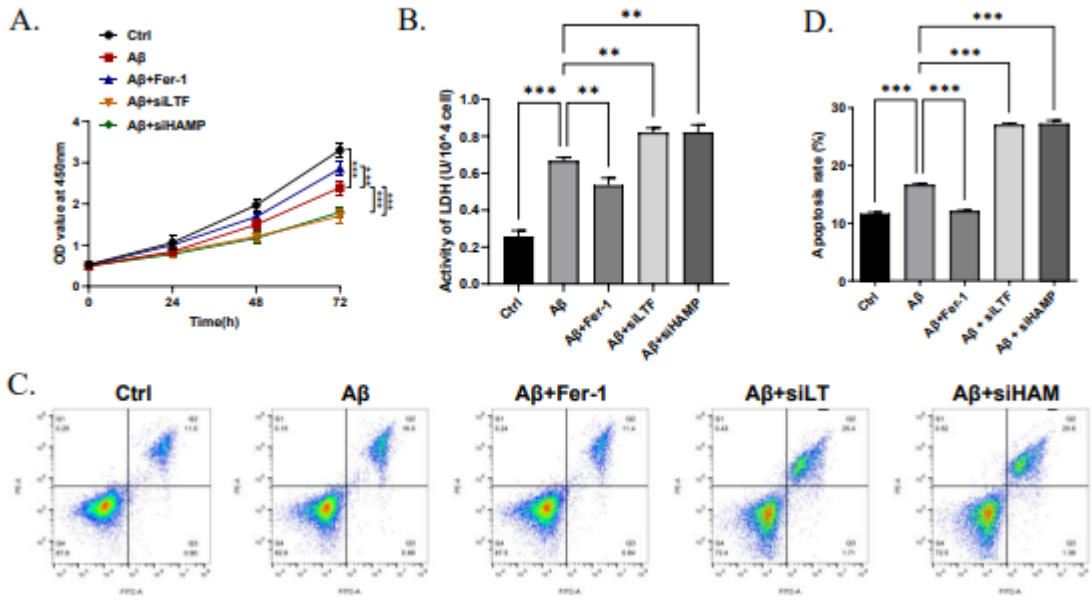

Figure 3. Cell viability and apoptosis analyses following LTF and HAMP knockdown in AD cell models. (A) OD values for different cell groups measured by CCK-8 assay. (B) LDH release levels assessed by LDH cytotoxicity assay. (C) Apoptotic status of different groups evaluated by flow cytometry. (D) Quantification of apoptosis rates based on flow cytometry results

DOI: 10.54254/2753-8818/2026.36010

3.4. LTF and HAMP modulate ferroptosis in AD cell models

To investigate the relationship between LTF and HAMP expression and neuronal ferroptosis in AD, we measured several ferroptosis-related indicators, including intracellular Fe^{2+} levels, mitochondrial morphology, MDA and GSH levels, as well as the expression of core regulatory genes in different SH-SY5Y cell groups.

As shown in Figure 4A, AD cell models (Aβ-treated) exhibited significantly increased intracellular Fe^{2+} levels, a critical requirement for ferroptosis, compared to normal SH-SY5Y cells. Treatment of the ferroptosis inhibitor Fer-1 partially reversed this increase, whereas siRNA-mediated knockdown of LTF or HAMP further elevated iron accumulation, indicating that both genes are involved in maintaining iron homeostasis.

Figure 4B illustrates mitochondrial morphology assessed by transmission electron microscopy (TEM). Normal SH-SY5Y cells displayed intact cristae, whereas AD models showed cristae loss, a hallmark of ferroptosis. Knockdown of LTF or HAMP exacerbated mitochondrial damage, with additional vacuolation or air/liquid bubble formation, suggesting impaired mitochondrial function and more severe ferroptotic stress.

We further assessed oxidative stress indicators. Malondialdehyde (MDA), a product of lipid peroxidation, significantly increased, and glutathione (GSH), an antioxidant that detoxifies lipid peroxides, markedly decreased in AD models compared to controls (Figure 4C). Fer-1 treatment partially restored MDA and GSH levels, whereas siRNA knockdown of LTF or HAMP aggravated the imbalance, supporting the involvement of these genes in regulating ferroptotic pathways.

Collectively, these results indicate that downregulation of LTF and HAMP in AD promotes iron accumulation, mitochondrial dysfunction, and lipid peroxidation, thereby enhancing neuronal ferroptosis.

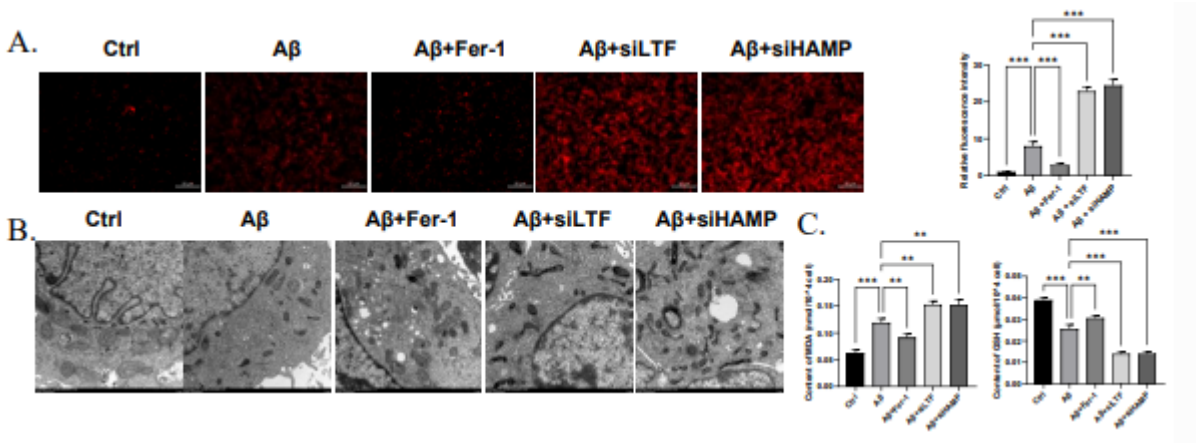

Figure 4. Assessment of intracellular Fe^{2+}, mitochondrial morphology, and oxidative stress markers. (A) Quantification of intracellular Fe^{2+} levels by FerroOrange staining and fluorescence microscopy (scale bar, 50 μm). (B) Transmission electron microscopy images illustrating mitochondrial intermembrane space changes. (C) Measurement of MDA and GSH levels using respective assay kits

3.5. LTF and HAMP regulate lipid ROS and cellular oxidative stress in AD

Lipid ROS serve as direct executors of ferroptotic cell death. A high ratio of oxidized to reduced lipid ROS drives lipid peroxidation, promoting ferroptosis, whereas reduced lipid ROS can inhibit

DOI: 10.54254/2753-8818/2026.36010

this process and protect cells. As shown in Figure 5A, AD cell models (Aβ-treated SH-SY5Y cells) exhibited a significantly higher oxidized/reduced lipid ROS ratio compared to normal SH-SY5Y cells, indicating enhanced ferroptotic stress. Treatment with the ferroptosis inhibitor Fer-1 reduced this ratio to near-normal levels, whereas siRNA-mediated knockdown of LTF or HAMP markedly increased it again. These results underscore the positive association between elevated lipid ROS and susceptibility to ferroptosis, and support the hypothesis that downregulation of LTF and HAMP exacerbates ferroptotic damage in AD neuronal models. Although total ROS levels are not direct triggers of ferroptosis, they reflect the cellular oxidative state and indicate an increased propensity for lipid ROS oxidation. Consistently, Figure 5B shows that the oxidized/reduced total ROS ratio follows a similar trend: it is elevated in AD models, reduced by Fer-1 treatment, and further increased upon LTF or HAMP knockdown.

Together, these findings highlight that LTF and HAMP are key modulators of ferroptosis, acting to restrain lipid ROS accumulation and oxidative stress in AD neuronal cells. Their downregulation in early AD contributes to increased ferroptotic vulnerability, providing a mechanistic link to neuronal loss.

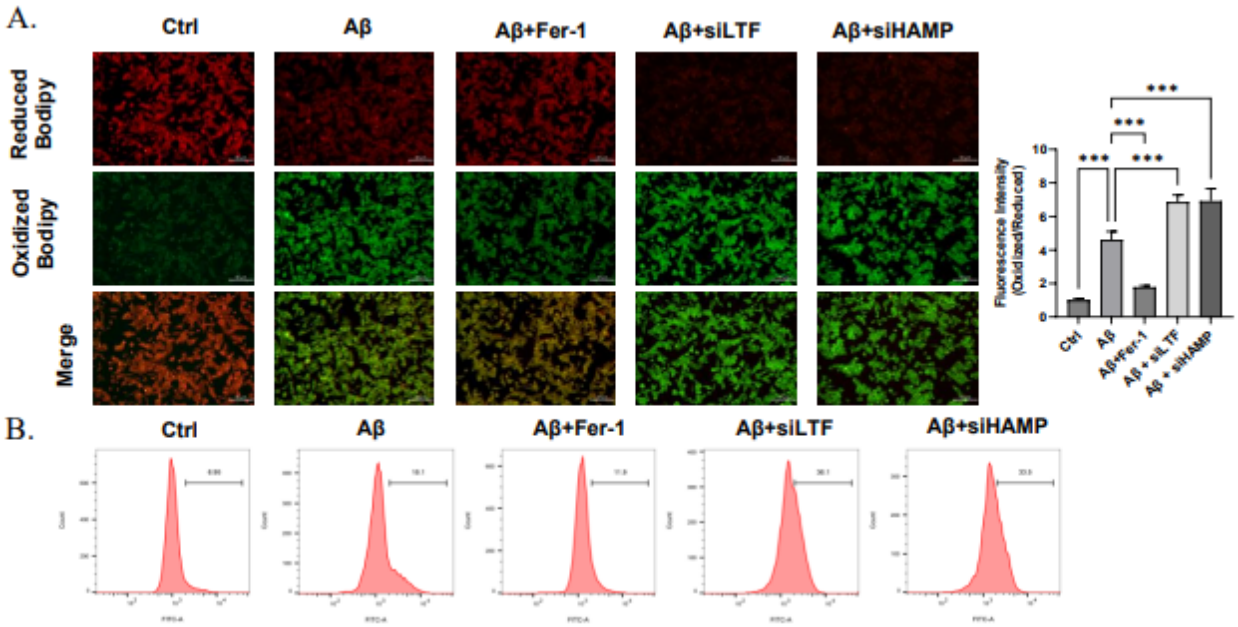

Figure 5. Effects of LTF and HAMP knockdown on ferroptosis-related indicators. (A) Quantification of oxidized/reduced lipid ROS ratios in various cell groups using a ROS detection probe and fluorescence microscopy. (B) Measurement of oxidized/reduced total ROS ratios among different cell groups, analyzed by flow cytometry

3.6. LTF and HAMP influence core ferroptosis regulatory genes in AD

GPX4, SLC7A11, and ACSL4 are central regulators of the ferroptosis pathway, controlling lipid peroxidation and neuronal ferroptosis. As shown in Figure 6, AD cell models (Aβ-treated SH-SY5Y cells) exhibited downregulation of GPX4 and SLC7A11 and upregulation of ACSL4 compared with normal SH-SY5Y cells, indicating enhanced ferroptotic activity.

Treatment with the ferroptosis inhibitor Fer-1 reversed these changes, restoring GPX4 and SLC7A11 levels while lowering ACSL4 expression, confirming its protective effect against ferroptosis. In contrast, siRNA-mediated knockdown of LTF or HAMP further suppressed GPX4

DOI: 10.54254/2753-8818/2026.36010

and SLC7A11 while elevating ACSL4 expression beyond the levels seen in AD models alone, indicating exacerbated ferroptotic stress.

These results support the conclusion that LTF and HAMP act as modulators of neuronal ferroptosis. Reduced expression of these genes in early AD contributes to enhanced ferroptotic damage, whereas their adequate expression mitigates ferroptosis and promotes neuronal survival. Therefore, LTF and HAMP may serve as potential therapeutic targets, and strategies to maintain or enhance their expression could protect neurons by suppressing ferroptosis in AD.

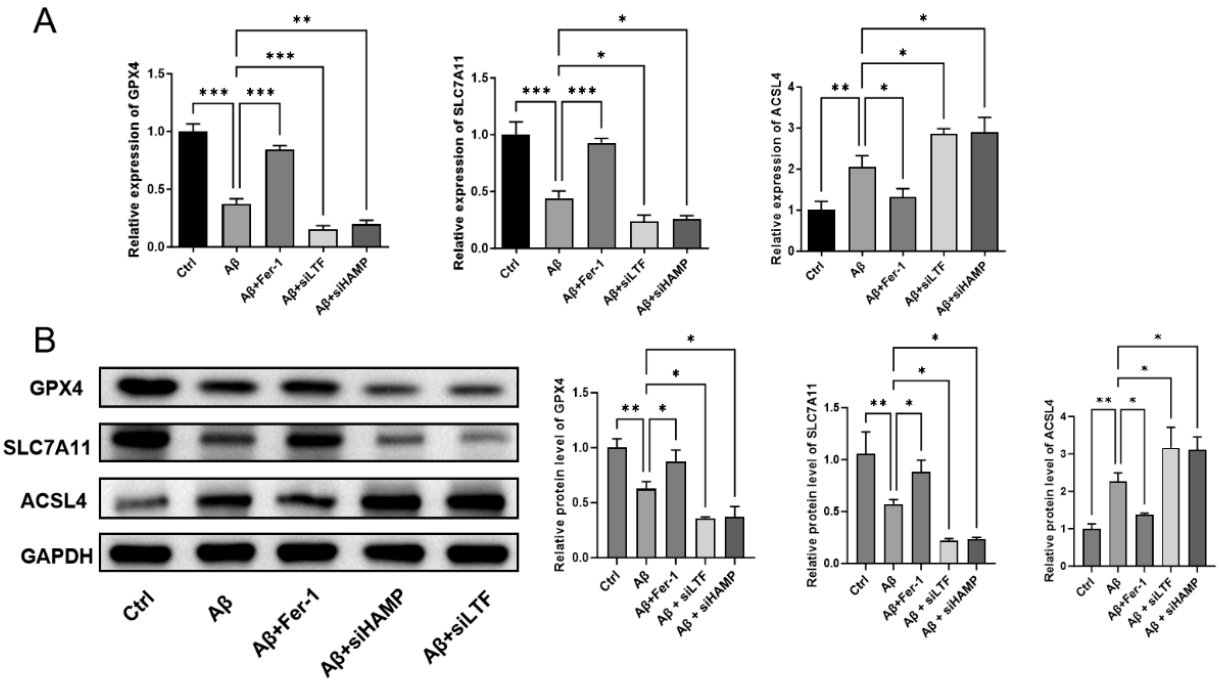

Figure 6. Expression of ferroptosis-associated marker genes. (A) Relative expression levels of GPX4, SLC7A11, and ACSL4 determined by quantitative real-time PCR. (B) Western blot images illustrating the expression of GPX4, SLC7A11, and ACSL4, with GAPDH as the loading control

4. Discussion

A major finding of this in vitro study is the role of LTF and HAMP on neuronal ferroptosis. LTF is a multifunctional iron-binding glycoprotein that chelates iron, reduces ROS, and mitigates oxidative stress, thereby protecting tissues, including the brain, from ferroptosis [24]. Bioinformatics and experimental validation further support LTF as a ferroptosis-related gene, modulating iron metabolism and oxidative stress responses critical for neuronal integrity in neurodegeneration [25]. HAMP (hepcidin antimicrobial peptide), encoded by the HAMP gene, is a central regulator of iron homeostasis, controlling iron flux across the blood-brain barrier via ferroportin on brain endothelial cells. Knockdown of astrocyte-derived hepcidin increases brain iron levels and induces cognitive decline, highlighting its neuroprotective function against iron toxicity and ferroptosis [26].

Previous studies suggest that in AD, astrocyte-derived lactoferrin protects neurons by reducing iron accumulation and lipid peroxidation while increasing GPX4 levels [27]. Similarly, decreased hepcidin and dysregulated iron metabolism correlate with iron deposition, elevated lipid peroxidation, and neuronal loss via ferroptosis in AD models and patients [28]. These findings are

DOI: 10.54254/2753-8818/2026.36010

consistent with our results showing that altered LTF and HAMP expression modulate ferroptotic severity in cell models. Interestingly, discrepancies emerge when comparing expression patterns between bioinformatics data and cell models. In the hippocampal samples from AD patients, both LTF and HAMP are upregulated, whereas in SH-SY5Y-based AD cell models, their expression is significantly reduced. This apparent contradiction can be explained by the dynamic, stage-dependent regulation of these genes in the human brain.

An explanation can be proposed to explain these seemingly contradictory results: the expression of LTF and HAMP experience changes throughout the AD continuum due to the negative feedback that contributes to maintaining homeostasis in the human body. We propose the following hypothesis: in early AD, Aβ accumulation suppresses LTF and HAMP expression in neurons, leading to Fe^{2+} accumulation, oxidative stress, and increased ferroptotic susceptibility. The seemingly contradictory expression patterns of LTF and HAMP between AD cell models and human hippocampal samples can be explained by stage-dependent regulation and negative feedback. In early AD, Aβ accumulation suppresses LTF and HAMP expression in neurons, leading to Fe^{2+} accumulation, oxidative stress, and increased susceptibility to ferroptosis, as observed in SH-SY5Y-based AD cell models. In vivo, however, compensatory mechanisms upregulate LTF and HAMP to partially restore iron homeostasis and mitigate ferroptotic damage. As AD progresses, this compensatory upregulation becomes pronounced, explaining the hyper-expression observed in post-mortem hippocampal samples from late-stage patients. Despite this, continued Fe^{2+} accumulation and oxidative stress eventually overwhelm neuronal defenses, resulting in ferroptosis.

This model reconciles differences between in vitro and in vivo observations and highlights the dynamic role of LTF and HAMP in neuronal ferroptosis. In cell models lacking systemic feedback, LTF and HAMP remain suppressed and ferroptosis occurs rapidly. In contrast, neurons in the human brain exhibit delayed ferroptosis due to compensatory upregulation. Overall, Aβ accumulation acts to inhibit LTF and HAMP, promoting ferroptosis, while the body responds via negative feedback. Ultimately, this compensatory increase is insufficient to prevent neuronal loss in late-stage AD. Future studies tracking LTF and HAMP expression throughout disease progression are warranted to validate this hypothesis and clarify their temporal role in ferroptosis regulation.

5. Conclusion

This study demonstrates that LTF and HAMP are critical modulators of neuronal ferroptosis in AD. Bioinformatics and in vitro analyses revealed that Aβ-induced suppression of LTF and HAMP in early AD promotes Fe^{2+} accumulation, oxidative stress, and ferroptotic cell death. Conversely, compensatory upregulation of these genes in vivo reflects a negative feedback mechanism aimed at mitigating ferroptosis, which explains their hyper-expression in late-stage AD hippocampal tissue. Knockdown experiments confirmed that reduced expression of LTF or HAMP exacerbates ferroptotic damage, while Fer-1 treatment restores iron homeostasis and cell viability. These findings provide mechanistic insights into the temporal regulation of neuronal ferroptosis, highlighting LTF and HAMP as potential therapeutic targets for AD intervention. Future studies should focus on longitudinal assessment of LTF and HAMP expression throughout disease progression to validate their protective roles.

Acknowledgement

A final thanks to my parents, for all the support they've given.

DOI: 10.54254/2753-8818/2026.36010

References

[1] Heneka, M. T., Morgan, D., & Jessen, F. (2024). Passive anti-amyloid β immunotherapy in Alzheimer's disease—opportunities and challenges. *The Lancet, 404*(1), 2198-2208.

[2] Scheltens, P., et al. (2021). Alzheimer's disease. *The Lancet, 397*(1), 1577-1590.

[3] Gustavsson, A., et al. (2023). Global estimates on the number of persons across the Alzheimer's disease continuum. *Alzheimer's & Dementia, 19*(1), 658-670.

[4] Alam, K., et al. (2024). Global burden of 288 causes of death and life expectancy decomposition in 204 countries and territories and 811 subnational locations, 1990-2021: A systematic analysis for the Global Burden of Disease Study 2021. *The Lancet (British edition)*.

[5] Nichols, E., et al. (2022). Estimation of the global prevalence of dementia in 2019 and forecasted prevalence in 2050: An analysis for the Global Burden of Disease Study 2019. *The Lancet Public Health, 7*(1), e105-e125.

[6] Hampel, H., et al. (2021). The amyloid-β pathway in Alzheimer's disease. *Molecular Psychiatry, 26*(1), 5481-5503.

[7] Wirths, O., & Zampar, S. (2020). Neuron loss in Alzheimer's disease: Translation in transgenic mouse models. *International Journal of Molecular Sciences, 21*, 8144.

[8] Jahn, H. (2013). Memory loss in Alzheimer's disease. *Dialogues in Clinical Neuroscience, 15*, 445-454.

[9] Mangalmurti, A., & Lukens, J. R. (2022). How neurons die in Alzheimer's disease: Implications for neuroinflammation. *Current Opinion in Neurobiology, 75*, 102575.

[10] Dixon, S. J., et al. (2012). Ferroptosis: An iron-dependent form of nonapoptotic cell death. *Cell, 149*, 1060-1072.

[11] Jiang, X., Stockwell, B. R., & Conrad, M. (2021). Ferroptosis: Mechanisms, biology and role in disease. *Nature Reviews Molecular Cell Biology, 22*, 266-282.

[12] Reichert, C. O., et al. (2020). Ferroptosis mechanisms involved in neurodegenerative diseases. *International Journal of Molecular Sciences, 21*, 8765.

[13] Bao, W.-D., et al. (2021). Loss of ferroportin induces memory impairment by promoting ferroptosis in Alzheimer's disease. *Cell Death & Differentiation, 28*(2), 1548–1562.

[14] Do Van, B., et al. (2016). Ferroptosis, a newly characterized form of cell death in Parkinson's disease that is regulated by PKC. *Neurobiology of Disease, 94*, 169–178.

[15] Wang, F., et al. (2022). Iron dyshomeostasis and ferroptosis: A new Alzheimer's disease hypothesis? *Frontiers in Aging Neuroscience, 14*, 830569.

[16] Jakaria, M., Belaidi, A. A., Bush, A. I., & Ayton, S. (2021). Ferroptosis as a mechanism of neurodegeneration in Alzheimer's disease. *Journal of Neurochemistry, 159*(2), 804–825.

[17] Yang, W. S., et al. (2014). Regulation of ferroptotic cancer cell death by GPX4. *Cell, 156*(1–2), 317–331.

[18] Koppula, P., Zhuang, L., & Gan, B. (2021). Cystine transporter SLC7A11/xCT in cancer: Ferroptosis, nutrient dependency, and cancer therapy. *Protein & Cell, 12*(8), 599–620.

[19] Anderson, M. E. (1985). Determination of glutathione and glutathione disulfide in biological samples. *Methods Enzymol, 113*, 548–555. https://doi.org/10.1016/s0076-6879(85)13073-9

[20] Yang, W. S., & Stockwell, B. R. (2016). Ferroptosis: Death by lipid peroxidation. *Trends in Cell Biology, 26*, 165–176.

[21] Doll, S., et al. (2017). ACSL4 dictates ferroptosis sensitivity by shaping cellular lipid composition. *Nature Chemical Biology, 13*, 91–98.

[22] Bustin, S. A., et al. (2009). The MIQE guidelines: Minimum information for publication of quantitative real-time PCR experiments. *Clinical Chemistry, 55*, 611–622. https://doi.org/10.1373/clinchem.2008.112797

[23] Burnette, W. N. (1981). "Western blotting": Electrophoretic transfer of proteins from sodium dodecyl sulfate-polyacrylamide gels to unmodified nitrocellulose and radiographic detection with antibody and radioiodinated protein A. *Analytical Biochemistry, 112*, 195–203.

[24] Wang, J., Xiu, M., Wang, J., Gao, Y., & Li, Y. (2024). METTL16-SENP3-LTF axis confers ferroptosis resistance and facilitates tumorigenesis in hepatocellular carcinoma. *Journal of Hematology & Oncology, 17*, 78. https://doi.org/10.1186/s13045-024-01599-6

[25] Zeng, C., et al. (2024). Identification and experimental validation of ferroptosis-related gene lactotransferrin in age-related hearing loss. *Frontiers in Aging Neuroscience, 16*, 1309115. https://doi.org/10.3389/fnagi.2024.1309115

[26] You, L., et al. (2022). Astrocyte-derived hepcidin controls iron traffic at the blood-brain-barrier via regulating ferroportin 1 of microvascular endothelial cells. *Cell Death & Disease, 13*, 667. https://doi.org/10.1038/s41419-022-05043-w

[27] Fan, Y. G., et al. (2024). Astrocyte-derived lactoferrin inhibits neuronal ferroptosis by reducing iron content and GPX4 degradation in APP/PS1 transgenic mice. *Pharmacological Research, 209*, 107404.

DOI: 10.54254/2753-8818/2026.36010

https://doi.org/10.1016/j.phrs.2024.107404

[28] Ashraf, A., Jeandriens, J., Parkes, H. G., & So, P. W. (2020). Iron dyshomeostasis, lipid peroxidation and perturbed expression of cystine/glutamate antiporter in Alzheimer's disease: Evidence of ferroptosis. *Redox Biology, 32*, 101494. https://doi.org/10.1016/j.redox.2020.101494